

Tracking contrast agents using real-time 2D photoacoustic imaging system for cardiac applications

Ragnar Olafsson^{*}, Leonardo Montilla, Pier Ingram, and Russell S. Witte.
Department of Radiology, University of Arizona,
1609 N Warren, Bldg 211, Tucson, AZ USA 85724

ABSTRACT

Photoacoustic (PA) imaging is a rapidly developing imaging modality that can detect optical contrast agents with high sensitivity. While detectors in PA imaging have traditionally been single element ultrasound transducers, use of array systems is desirable because they potentially provide high frame rates to capture dynamic events, such as injection and distribution of contrast in clinical applications. We present preliminary data consisting of 40 second sequences of co-registered pulse-echo (PE) and PA images acquired simultaneously in real time using a clinical ultrasonic machine. Using a 7 MHz linear array, the scanner allowed simultaneous acquisition of inphase-quadrature (IQ) data on 64 elements at a rate limited by the illumination source (Q-switched laser at 20 Hz) with spatial resolution determined to be 0.6 mm (axial) and 0.4 mm (lateral). PA images had a signal-to-noise ratio of approximately 35 dB without averaging. The sequences captured the injection and distribution of an infrared-absorbing contrast agent into a cadaver rat heart. From these data, a perfusion time constant of 0.23 s^{-1} was estimated. After further refinement, the system will be tested in live animals. Ultimately, an integrated system in the clinic could facilitate inexpensive molecular screening for coronary artery disease.

Keywords: photoacoustic, optoacoustic, ultrasound, coronary heart disease, perfusion imaging, contrast agents, molecular imaging

1. INTRODUCTION

In its infancy photoacoustic (PA) imaging was performed using mechanically scanned single element ultrasound transducers¹. Due to the slow scanning speed of these systems, there has been considerable effort to implement ultrasound receiving arrays for data capture. These arrays are typically modified ultrasound scanners or custom systems. Groups using custom hardware have been able to show high frame rate PA imaging from 15-50 Hz. However, in these studies co-registered pulse echo (PE) ultrasound images have not been acquired simultaneously²⁻⁴. These ultrasound scanners have been limited to frame rates less than 1 Hz, primarily because they lacked parallel receive architecture and access to pre-beamformed data.⁵⁻⁷ Other systems demonstrated PA imaging co-registered with static PE images at a relatively high frame rate ($\sim 10\text{Hz}$)⁸⁻¹⁰. In this paper we describe the acquisition of real time co-registered PA and PE imaging sequences using a clinical ultrasonic machine (z.one, Zonare Medical Systems, Mountainview, CA). We implemented the system to dynamically track the perfusion of an infrared-absorbing contrast agent in an excised rat heart with the ultimate aim of developing novel screening methods for coronary heart disease based on photoacoustic imaging.

According to the American Heart Association approximately 1200 U.S. Citizens die each year from coronary heart disease (CHD) with an estimated cost of CHD close to \$156.4 billion in 2008¹¹ and an average cost of a diagnostic test approaching \$30,000. Thus, there is an enormous incentive for creating new, quick, and cost effective ways to screen for and diagnose CHD at the earliest stage possible.

Imaging diagnostic methods for CAD can be classified into three main groups; gross anatomical, untargeted contrast imaging, and targeted contrast imaging. The main two gross anatomical methods are stress echocardiography and multidetector row computed tomography (MCT). MCT has been used to detect and quantify coronary calcification, an indirect measure of atherosclerosis. This is primarily useful in younger patients since the coronaries of older individuals tend to be calcified to some extent¹². In stress echocardiography, an image taken during resting condition is compared to images taken under physiological stress, induced with either exercise or drugs (e.g. dobutamine). The increased demand created with the stress cannot be met by underperfused muscles, causing them to contract less. This abnormal muscle contraction presents itself in so-called "abnormal wall motion," as estimated by the radiographer¹³. A number of research groups are working to improve on this method by estimating the abnormal motion with ultrasonic strain imaging¹⁴⁻¹⁷.

X-ray angiography, for which radiopaque material is injected with a catheter into the coronaries, remains the gold standard for diagnosing coronary vessel constriction with untargeted contrast. The coronary tree is then scanned for abnormalities and constrictions¹⁸. Although it has good spatial resolution and can help identify constricted vessels, it does not measure perfusion, thereby allowing the possibility that a myocardium fed by a constricted coronary can be fed by parallel circulation¹⁹. Methods that measure perfusion directly are single photon emission computed tomography (SPECT), magnetic resonance imaging (MRI), and myocardial contrast echocardiography (MCE)^{20, 21}. An indicator is injected in a stress protocol similar to what is described above. Any myocardial region that does not “light up” with contrast agent is scrutinized. MRI has been used less because of its greater cost. SPECT and MCE have been shown to offer similar performance in terms of specificity and sensitivity, but MCE has higher spatial resolution and does not incur radiation dose²².

The third and final class is targeted contrast imaging. In this regime, the contrast agents have biomarkers that bind specifically to early indicators of atherosclerosis, such as inflammation and fibrosis. The main modality so far has been SPECT, but there are efforts to develop targeted ultrasound and MRI contrast²³⁻²⁵.

Photoacoustic imaging could have a niche as a screening method by enhancing traditional ultrasound contrast. Photoacoustics has been used to image cardiovascular dynamics in murine hearts⁴ and to characterize vulnerable plaques using intravascular ultrasonic (IVUS) catheters^{26, 27}. Perfusion imaging has been also demonstrated,^{6, 28, 29} as well as contrast agents targeting vascular inflammation²⁶. We envision a potential molecular photoacoustic imaging system for screening early indicators of coronary heart disease, with special emphasis on imaging the proximal coronaries.³⁰

2. METHODS AND MATERIALS

The experimental setup is shown in Fig. 1. A cadaver rat heart was suspended inside a watertank. The watertank had an acoustic window at the bottom and an optical window on the side. A 7 MHz ultrasonic linear array (L10-5, Zonare Medical Systems, Mountain View, CA) was placed under the heart against the gel-coupled acoustic window. The linear array was connected to a clinical ultrasound scanner (z.one, Zonare Medical Systems, Mountain View, CA). As depicted in Fig. 1, the lateral and axial scanner coordinates define the x and z coordinate axis while the y -axis is perpendicular to the imaging plane. The linear array had 128 elements; each element had dimensions of 0.3 mm (azimuthal) and 5 mm (elevational). The z.one scanner acquires and stores inphase-quadrature (IQ) data on 64 elements simultaneously, such that full 2D photoacoustic frames can be acquired with a single laser firing. At 20 Hz frame rate, the memory of the z.one scanner can store up to 70 second (1400) long sequences. The data was downloaded through ethernet protocol to an external personal computer (PC).

Illumination was provided by a wavelength-tunable laser system. An optical parametric oscillator (Surelite OPO, Continuum II-20) was pumped by a frequency-doubled Q-switched (QS) laser (5 ns pulse width; Surelite I-20, Continuum Inc., Santa Clara, CA). The output of the system was tuned to 825 nm for this study. Light was directed in free space through a cylindrical lens (25.4 mm wide, focal length 38.1 mm) and a ground glass diffuser such that it generated a rectangular pattern (12.5 mm x 3 mm)--co-planar with the imaging plane of the linear array. The energy of each light pulse was approximately 20 mJ. Synchronization between the z.one scanner and the QS laser was provided by a field programmable gate array (FPGA) chip (ezFPGA; Dallas Logic, Plano, Texas). The frame rate of the scanner was limited by the pulse repetition rate of the laser (20 Hz). Spatial resolution of the photoacoustic imaging system was measured by placing a human hair inside the tank at the same location along the z -axis as the heart.

Solutions of different concentrations of contrast material (India Ink) were prepared by diluting it with deionized water (2000, 1000, 500, 200, 100, 50 parts per million (ppm)). The linearity of the photoacoustic signal with concentration was examined inside tubing (0.5 mm inner diameter) placed at the same imaging depth as the cadaver heart. The absorbance as a function of concentration was independently measured using an optical transmission spectrometer (USB4000, Ocean Optics, Dunedin, FL).

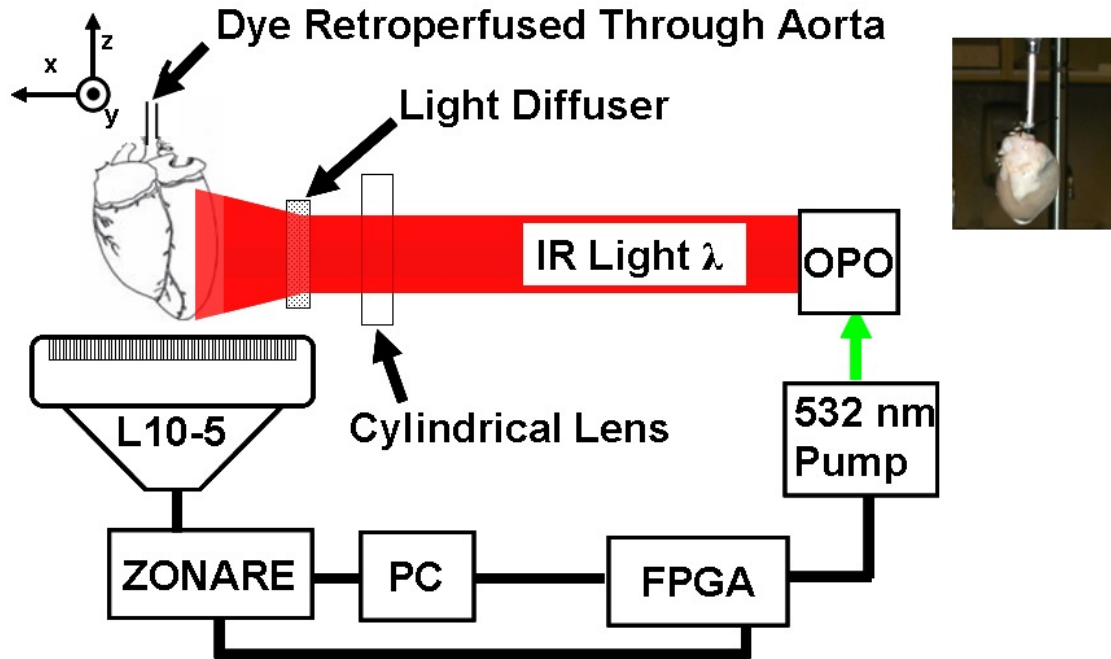


Figure 1: Experimental setup. A cadaver rat heart (photographed in the upper right corner) was placed inside a water tank filled with de-ionized water. The experiment was controlled by a computer (PC) through Matlab™ with a field programmable gate array (FPGA) to control timing. A 532 nm Q-switched laser, triggered by the FPGA at 20 Hz, pumped an optical parametric oscillator (OPO) to produce infrared light (IR) of wavelength λ . The IR light illuminating the heart was focused into a line pattern using a cylindrical lens and diffused with ground glass. The photoacoustic emission was measured by a linear array (L10-5) and an ultrasound scanner (Zonare).

To test the scanner, contrast material (India ink) was injected into the heart with a syringe pump (2400-006, Harvard Apparatus, Holliston, MA) at 2 ml/min via a cannula placed into the aorta. For each injection, IQ data was acquired for 40 seconds. Pulse echo data were acquired concurrently with the PA data by programming the scanner to transmit a plane wave at the same time as the laser firing. PA images and PE images were formed from IQ data using delay and sum beamforming based on one way and two way propagation, respectively. After each injection of contrast, deionized water was injected for 2 minutes to wash out any remaining contrast material.

3. RESULTS

We have demonstrated real time acquisition of PA images co-registered with PE ultrasound using a clinical ultrasound scanner. The scanner was used to dynamically track the injection of PA contrast material into a cadaver rat heart.

Figure 2 depicts a PA wavefield and beamformed PA image of a human hair that was analyzed to estimate the spatial resolution of the system at the same imaging depth as the cadaver heart. The beamformed image has a dynamic range of 60dB and a characteristic “bow-tie” beamforming artifact. At -6 dB the resolution was 0.4 mm laterally and 0.6 mm axially.

The results of the spectrographic characterization of the ink are shown in Fig. 3. The figure demonstrates that the contrast material had a relatively flat absorption spectrum in the near infrared spectrum. It also demonstrates the linearity of contrast absorbance with concentration with good agreement with the amplitude of the photoacoustic signal (Figure 4).

Figure 5 presents results of the injection of diH₂O water (0 ppm solution) into the heart. The first frame of a 40-second sequence is depicted (A), representing a pulse-echo image (grayscale) co-registered with the PA image (hot scale) collected simultaneously. In these images, the heart is illuminated from the left; The strong background PA signal is due to higher fluence at that side of the heart. The cannula is seen as a blip in the PA image and a bright spot in the PE image near coordinate $(x,z) = (10, 28.5)$ mm. The distention of the heart due to the injection is seen on the left (M-mode image of line $z=28.5$ mm) after approximately 10 seconds (B). The slow time PA signal (C) corresponding to the vertical dotted line in (B) illustrates the temporal evolution of the PA signal from the cannula. The large abrupt discontinuous changes

are due to bubbles in the water stream that mask the light and the sound. There is a slower evolution of ~6-8 dB, which is more difficult to interpret, but some change is expected due to geometrical distortions of the distending heart.

Figure 6 depicts results of an injection of 10 ppm solution. There was a 30 dB increase in signal amplitude as a function of time in an area near the base of the heart. This increase is demonstrated in the M-mode image (B) from the line $z = 27$ mm and the PA slow time trace (C). Assuming an exponential model, a ten second increase produces a 20 dB (tenfold) change in signal amplitude with an equivalent time constant of 0.23 s^{-1} .

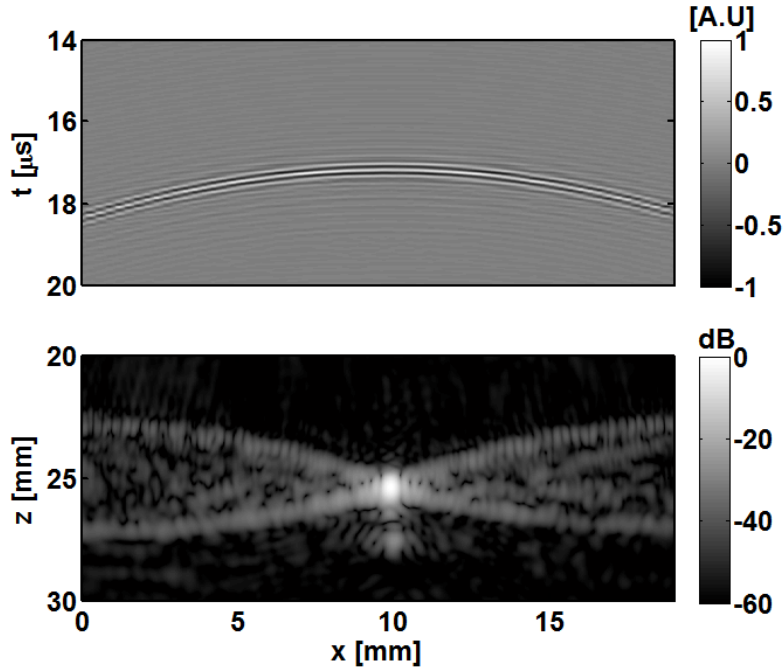


Figure 2: Top: Photoacoustic wavefield emitted from a human hair. The colorscale is in arbitrary units (A.U.). Bottom: The beamformed photoacoustic image of the human hair. The -6dB resolution measured 0.6 mm axially and 0.4 mm laterally.

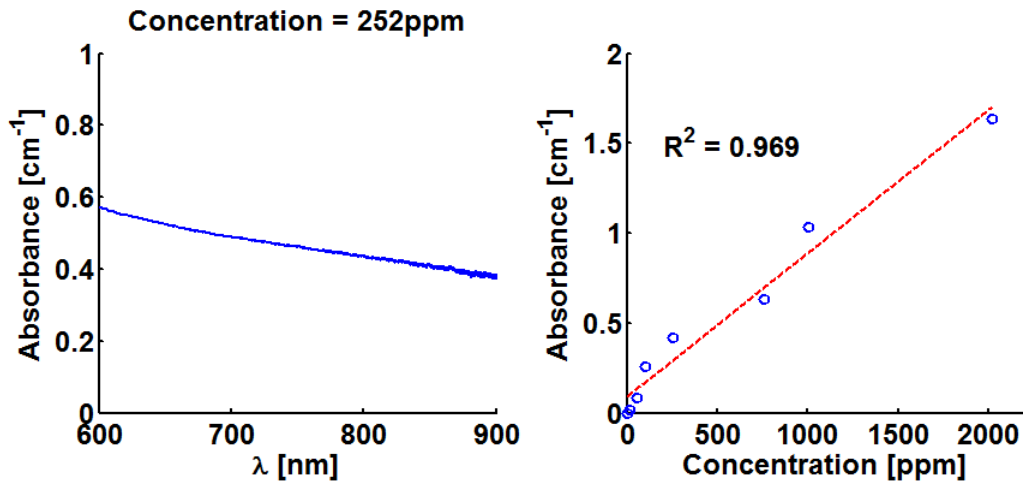


Figure 3: Left: A representative absorbance spectrum of the contrast material. Right: The absorbance at 825 nm of the contrast material as a function of concentration.

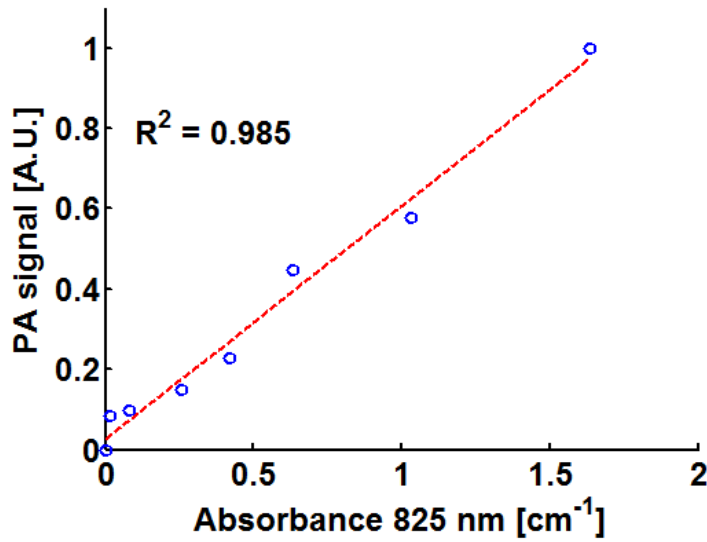


Figure 4: Comparison of photoacoustic signal amplitude and spectroscopic measurements for different concentrations of India ink.

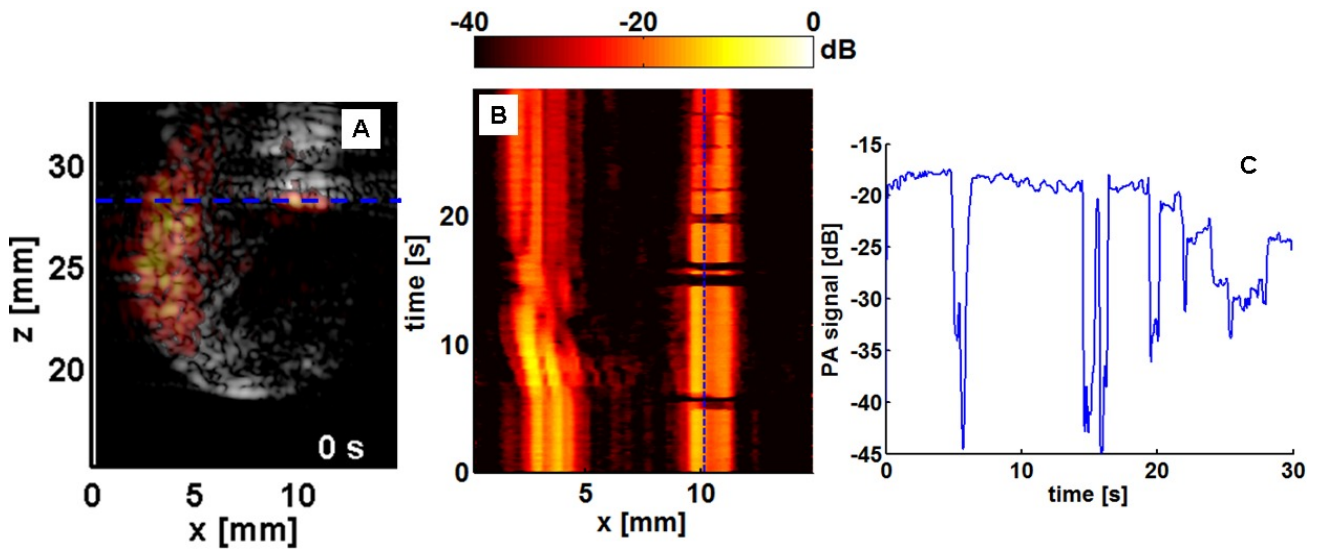


Figure 5: Injection of 0 ppm solution (deionized water) into heart. *A*) The first frame in a movie sequence captured during the injection. The pulse echo (PE) image is shown in gray scale on a 40 dB dynamic range. The photoacoustic (PA) image is superimposed in hot scale of 40 dB with 60% transparency. *B*) An M-mode PA image corresponding to the blue dashed line ($z = 28.5$ mm) in *A*). This line transects the photoacoustic signal of the cannula seen in *A*). The vertical blue dashed line is shown as plot in *C*).

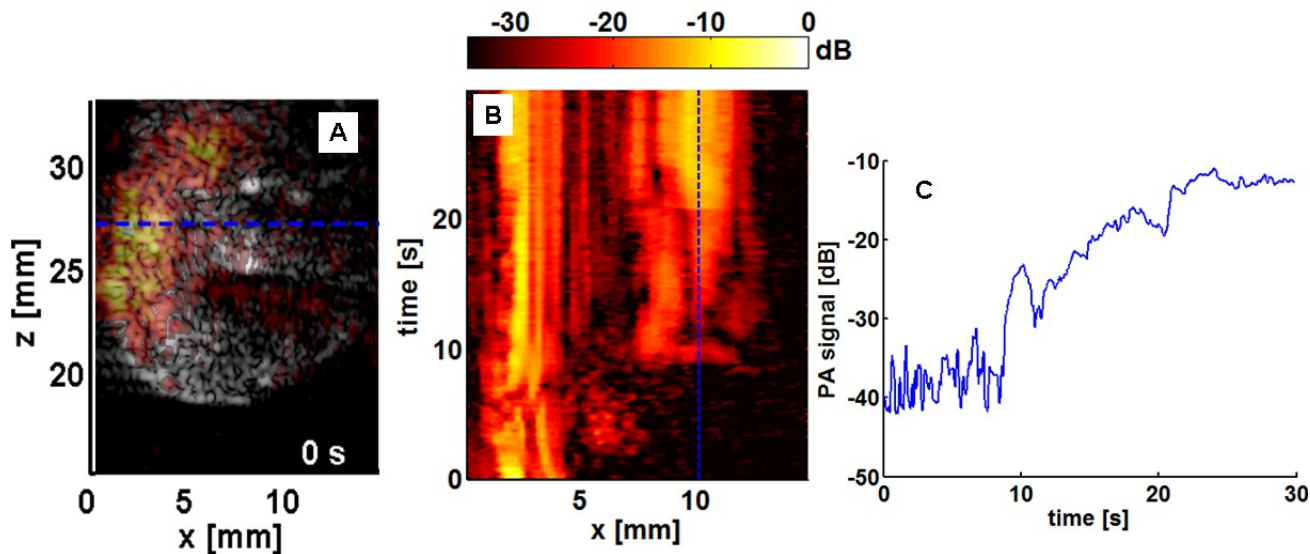


Figure 6: Injection of 10 ppm solution into heart. *A)* The first frame in movie sequence captured during the injection. The pulse echo (PE) image is shown in gray scale on a 40 dB dynamic range. The photoacoustic (PA) image is superimposed in hot scale of 40 dB with 60% transparency. *B)* An M-mode PA image corresponding to the blue dashed line ($z = 27$ mm) in *A)*. The vertical blue dashed line is shown as plot in *C)*.

4. DISCUSSION

The results presented in this paper demonstrate the use of real time acquisition of co-registered pulse-echo and photoacoustic images using a clinical ultrasonic scanner. The scanner was used to track the injection of photoacoustic contrast material into a cadaver rat heart.

Though preliminary, these results are very encouraging. It was possible to detect the injection of a low concentration (10 ppm) of contrast material and to estimate a perfusion constant of 0.23 s^{-1} . Some part of the change seen in Fig. 6 *C)* was due to the heart distending during injection. However, given the relatively small motion of the base of the heart (where the contrast material appears) in the co-registered pulse-echo image, the effect of this distention is likely negligible. The utility of co-registered pulse-echo images was also apparent for explaining the discontinuities in the PA signal in Fig. 5 *B)* and *C)*. Air bubbles coming through the aortic cannula had very bright PE signatures and their arrival coincided with the disruptions in PA signal.

A number of future improvements will be made to the system. The bow tie beamforming artifact seen in the image of the hair (Fig. 2) will be reduced with improved beamforming, such as apodization. Large background signal can be seen in Figs. 5 and 6 on the side of the heart facing the illumination source. Due the heart distending and changing shape during the injection, naïve subtraction of background was not possible. Motion compensation using the PE signals will enable background subtraction and improve visualization of myocardial perfusion. The non-uniform distribution of the PA signal due to the asymmetric distribution of illumination can also be seen in Fig. 5 and 6. This can be improved, for example, by omni-directional illumination or adding light scatters to the medium surrounding the heart.

The experimental setup was based on a Langendorff isolated heart setup, in which excised hearts are maintained alive for several hours through retroperfusion of the coronaries via the aorta³¹. This is made possible by the unidirectional properties of the aortic valve, which only admits flow away from the ventricle. In our setup it appears that the aortic valve had been breached because, in Fig. 5, air bubbles could be seen streaming through the cannula into the ventricle. Normally this setup is used with freshly excised hearts from animals infused with blood thinners. The cadaver heart was not freshly excised, so the coronaries could have been blocked, thereby impeding myocardial perfusion and increasing transvalvular pressure. The valve may also have been damaged due to handling and/or natural deterioration.

There may be advantages of photoacoustics over prevailing methods for perfusion imaging. Not only is PA imaging potentially four dimensional (3D space + time) with sub-mm spatial resolution, but also with a strong IR absorbing contrast agent, sensitivity might be better than microbubble-enhanced echocardiography or fluorescent imaging with

indocyanine green (Cardiac Green). In addition, while these preliminary studies exploit an untargeted dye, one long-term goal is to develop a non-invasive screening technique using molecular probes targeted to early disease markers, such as inflammation. Over the last decade, there has been considerable development of cardiac molecular imaging using SPECT and PE ultrasound. Photoacoustic screening based on a system described in this study potentially provides 3D perfusion imaging co-registered with pulse echo and blood flow ultrasound modalities. Unlike enhanced PE imaging, which is limited to endothelial targets due to size of microbubbles, PA nanoscale contrast agents could target a wider range of biomarkers--both intracellular and extracellular.

5. CONCLUDING REMARKS

We have described the use of clinical ultrasonic scanner for real time, co-registered photoacoustic and ultrasound imaging. After further refinement this flexible system will be applied to a variety of *in-vivo* and *in-vitro* studies, in particular molecular imaging of the cardiovascular system.

6. ACKNOWLEDGEMENTS

We would like to acknowledge the support and assistance of Zonare Medical Systems, the Advanced Research Institute for Biomedical Imaging (ARIBI), the Technology Research Infrastructure Fund (TRIF), Department of Radiology at the University of Arizona, and the Arizona Cancer Center. We would also like to thank Michael Bernas and Sarah Daley for their generous help and assistance with the setup.

REFERENCES

1. X. D. Wang, Y. J. Pang, G. Ku *et al.*, "Noninvasive laser-induced photoacoustic tomography for structural and functional in vivo imaging of the brain," *Nature Biotechnology*, 21(7), 803-806 (2003).
2. C. K. Liao, S. W. Huang, C. W. Wei *et al.*, "A high frame rate photoacoustic imaging system and its applications to perfusion measurements - art. no. 60860S," 7th Conference on Biomedical Thermoacoustics, Optoacoustics, and Acousto-Optics, S860-S860 (2006).
3. J. J. Niederhauser, M. Jaeger, R. Lemor *et al.*, "Combined ultrasound and optoacoustic system for real-time high-contrast vascular imaging in vivo," *IEEE Transactions on Medical Imaging*, 24(4), 436-440 (2005).
4. R. J. Zemp, L. A. Song, R. Bitton *et al.*, "Realtime photoacoustic microscopy in vivo with a 30-MHz ultrasound array transducer," *Optics Express*, 16(11), 7915-7928 (2008).
5. S. Park, S. R. Aglyamov, and S. Y. Emelianov, "Beamforming for photoacoustic imaging using linear array transducer," 2007 IEEE Ultrasonics Symposium, 856-859 (2007).
6. R. S. Witte, K. Kim, A. Ashish *et al.*, "Enhanced photoacoustic neuroimaging with gold nanorods and PEBBLEs - art. no. 685614," *Photons Plus Ultrasound: Imaging and Sensing 2008: the Ninth Conference on Biomedical Thermoacoustics, Optoacoustics, and Acoustic-Optics*, 6856, 85614-85614 (2008).
7. D. W. Yang, D. Xing, S. H. Yang *et al.*, "Fast full-view photoacoustic imaging by combined scanning with a linear transducer array," *Optics Express*, 15(23), 15566-15575 (2007).
8. L. Jankovic, K. Shahzad, Y. Wang *et al.*, "In Vivo Photoacoustic Imaging of Nude Mice Vasculature Using a Photoacoustic Imaging System Based on a Commercial Ultrasound Scanner," *Photons Plus Ultrasound: Imaging and Sensing 2008: The Ninth conference on Biomedical Thermoacoustics, Optoacoustics, and Acousto-optics*, 6856, 68560N-1 (2008).
9. R. G. M. Kolkman, P. J. Brands, W. Steenbergen *et al.*, "Real-time in vivo photoacoustic and ultrasound imaging," *Journal of Biomedical Optics*, 13(5), (2008).
10. Y. G. Zeng, D. Xing, Y. Wang *et al.*, "Photoacoustic and ultrasonic coimage with a linear transducer array," *Optics Letters*, 29(15), 1760-1762 (2004).
11. W. Rosamond, K. Flegal, K. Furie *et al.*, "Heart disease and stroke statistics - 2008 update - A report from the American Heart Association Statistics Committee and Stroke Statistics Subcommittee," *Circulation*, 117(4), E25-E146 (2008).
12. A. H. Mahnken, G. Muhlenbruch, R. W. Gunther *et al.*, "Cardiac CT: coronary arteries and beyond," *European Journal of Radiology*, 17, 994-1008 (2007).

13. M. L. Geleijnse, B. J. Krenning, A. Nemes *et al.*, "Diagnostic value of dobutamine stress echocardiography in patients with normal wall motion at rest," *Echocardiography-a Journal of Cardiovascular Ultrasound and Allied Techniques*, 24(5), 553-557 (2007).
14. C. Cianfrocca, F. Pelliccia, V. Pasceri *et al.*, "Strain rate analysis and levosimendan improve detection of myocardial viability by dobutamine echocardiography in patients with post-infarction left ventricular dysfunction: A pilot study," *Journal of the American Society of Echocardiography*, 21(9), 1068-1074 (2008).
15. A. Elen, H. F. Choi, D. Loeckx *et al.*, "Three-Dimensional Cardiac Strain Estimation Using Spatio-Temporal Elastic Registration of Ultrasound Images: A Feasibility Study," *IEEE Transactions on Medical Imaging*, 27(11), 1580-1591 (2008).
16. C. B. Ingul, E. Rozis, S. A. Slordahl *et al.*, "Incremental value of strain rate imaging to wall motion analysis for prediction of outcome in patients undergoing dobutamine stress echocardiography," *Circulation*, 115(10), 1252-1259 (2007).
17. C. Jia, R. Olafsson, K. Kim *et al.*, "2D Cardiac Elasticity Imaging on a Controlled Isolated Rabbit Heart," *Ultrasound in Medicine & Biology*, In submission, (2008).
18. R. M. Fleming, "Coronary artery disease is more than just coronary lumen disease," *American Journal of Cardiology*, 88(5), 599-600 (2001).
19. S. Kaul, "Coronary angiography cannot be used to assess myocardial perfusion in patients undergoing reperfusion for acute myocardial infarction," *Heart*, 86, 483-484 (2001).
20. H. Leong-Poi, E. Le, S. J. Rim *et al.*, "Quantification of myocardial perfusion and determination of coronary stenosis severity during hyperemia using real-time myocardial contrast echocardiography," *Journal of the American Society of Echocardiography*, 14(12), 1173-1182 (2001).
21. L. Claassen, G. Seidel, and C. Algermissen, "Quantification of flow rates using harmonic grey-scale imaging and an ultrasound contrast agent: an in vitro and in vivo study," *Ultrasound in Medicine and Biology*, 27(1), 83-88 (2001).
22. F. Xie, J. Hankins, H. A. Mahrous *et al.*, "Detection of Coronary Artery Disease with a Continuous Infusion of Definity Ultrasound Contrast during Adenosine Stress Real Time Perfusion Echocardiography," *Echocardiography-a Journal of Cardiovascular Ultrasound and Allied Techniques*, 24(10), 1044-1050 (2007).
23. H. F. Langer, R. Haubner, B. J. Pichler *et al.*, "Radionuclide imaging - A molecular key to the atherosclerotic plaque," *Journal of the American College of Cardiology*, 52(1), 1-12 (2008).
24. J. C. Wu, F. M. Bengel, and S. S. Gambhir, "Cardiovascular molecular imaging," *Radiology*, 244(2), 337-355 (2007).
25. A. P. Miller, and N. C. Nanda, "Contrast Echocardiography: New Agents," *Ultrasound in Medicine & Biology*, 30(4), 425-434 (2004).
26. K. Kim, S. W. Huang, S. Ashkenazi *et al.*, "Photoacoustic imaging of early inflammatory response using gold nanorods," *Applied Physics Letters*, 90(22), (2007).
27. S. Sethuraman, J. H. Amirian, S. H. Litovsky *et al.*, "Spectroscopic intravascular photoacoustic imaging to differentiate atherosclerotic plaques," *Optics Express*, 16(5), 3362-3367 (2008).
28. C. K. Liao, S. W. Huang, C. W. Wei *et al.*, "Nanorod-based flow estimation using a high-frame-rate photoacoustic imaging system," *Journal of Biomedical Optics*, 12(6), (2007).
29. S. Mallidi, A. B. Karpouk, S. R. Aglyamov *et al.*, "Measurement of blood perfusion using photoacoustic, ultrasound and strain imaging - art. no. 643707," 8th Conference on Biomedical Thermoacoustics, Optoacoustics and Acousto-optics, 43707-43707 (2007).
30. J. C. Wang, S. L. T. Normand, L. Mauri *et al.*, "Coronary artery spatial distribution of acute myocardial infarction occlusions," *Circulation*, 110(3), 278-284 (2004).
31. E. J. Tanhehco, K. Yasojima, P. L. McGeer *et al.*, "Free radicals upregulate complement expression in rabbit isolated heart," *American Journal of Physiology-Heart and Circulatory Physiology*, 279(1), H195-H201 (2000).